# eNeuro

### Research Article: New Research | Sensory and Motor Systems

### Odor concentration change coding in the olfactory bulb

Ana Parabucki<sup>1</sup>, Alexander Bizer<sup>1</sup>, Genela Morris<sup>1</sup>, Antonio E. Munoz<sup>2</sup>, Avinash D. S. Bala<sup>2</sup>, Matthew Smear<sup>2,3</sup> and Roman Shusterman<sup>1,2</sup>

<sup>1</sup>Sagol Department of Neurobiology, University of Haifa, Haifa, 3498838, Israel
 <sup>2</sup>Institute of Neuroscience, University of Oregon, Eugene, OR, 97403, USA
 <sup>3</sup>Department of Psychology, University of Oregon, Eugene, OR 97403, USA

https://doi.org/10.1523/ENEURO.0396-18.2019

Received: 14 October 2018

Revised: 4 January 2019

Accepted: 16 January 2019

Published: 1 February 2019

A.P. and R.S. conceptualized the study; A.B. and R.S. developed concentration change manifold; A.P. performed electrophysiological experiments; T.M. and A.D.S.B performed behavioral experiments; R.S. analyzed the data; G.M., M.S., and R.S. interpreted the data; G.M., M.S. and R.S. wrote the manuscript.

Funding: http://doi.org/10.13039/501100004963EC | Seventh Framework Programme (FP7) 334341

Funding: http://doi.org/10.13039/100000055HHS | NIH | National Institute on Deafness and Other Communication Disorders (NIDCD) R56DC015584 R56DC015584

Funding: http://doi.org/10.13039/501100003977Israel Science Foundation (ISF) 816/14 2212/14

### Conflict of Interest: No

Israel Science Foundation grants 816/14 and 2212/14 (R.S)

Marie Curie Career Integration grant 334341 (R.S.)

NIH/NICDC grants: R56DC015584 (R.S. and M.S.)

Correspondence should be addressed to Matthew Smear smear@uoregon.edu and Roman Shusterman, roma.shusterman@gmail.com

Cite as: eNeuro 2019; 10.1523/ENEURO.0396-18.2019

Alerts: Sign up at www.eneuro.org/alerts to receive customized email alerts when the fully formatted version of this article is published.

Accepted manuscripts are peer-reviewed but have not been through the copyediting, formatting, or proofreading process.

Copyright © 2019 Parabucki et al.

This is an open-access article distributed under the terms of the Creative Commons Attribution 4.0 International license, which permits unrestricted use, distribution and reproduction in any medium provided that the original work is properly attributed.

Manuscript title: Odor concentration change coding in the olfactory bulb Abbreviated title: deltaC coding in the olfactory bulb

### List all author names and affiliations:

Ana Parabucki<sup>1</sup>, Alexander Bizer<sup>1</sup>, Genela Morris<sup>1</sup>, Antonio E. Munoz<sup>2</sup>, Avinash D. S. Bala<sup>2</sup>, Matthew Smear<sup>2</sup>, <sup>3+</sup>, Roman Shusterman<sup>1, 2+</sup>

<sup>1</sup> Sagol Department of Neurobiology, University of Haifa, Haifa 3498838, Israel

<sup>2</sup> Institute of Neuroscience, University of Oregon, Eugene, OR 97403, USA

<sup>3</sup> Department of Psychology, University of Oregon, Eugene, OR 97403, USA

### Author contributions:

A.P. and R.S. conceptualized the study; A.B. and R.S. developed concentration change manifold; A.P. performed electrophysiological experiments; T.M. and A.D.S.B performed behavioral experiments; R.S. analyzed the data; G.M., M.S., and R.S. interpreted the data; G.M., M.S. and R.S. wrote the manuscript.

### Correspondence should be addressed to:

Matthew Smear smear@uoregon.edu and Roman Shusterman: roma.shusterman@gmail.com

Number of Figures: 7	Number of words for Abstract: 157
Number of Tables: 1	Number of words for Significance: 57
Number of Multimedia: 0	Number of words for Introduction: 337
	Number of words for Discussion: 1125

### Acknowledgments

We would like to acknowledge Yashar Ahmadian, and members of the Smear and Shusterman laboratories for discussions, Wolfgang Kelsch, Shawn Lockery, David McCormick, Kathy Nagel, Shy Shoham and Mike Wehr for comments on the manuscript.

Conflict of interest: No

### **Funding sources:**

Israel Science Foundation grants 816/14 and 2212/14 (R.S) Marie Curie Career Integration grant 334341 (R.S.) NIH/NICDC grants: R56DC015584 (R.S. and M.S.)

### 1 Summary

2 Dynamic changes in the environment strongly impact our perception. Likewise, sensory systems preferentially represent stimulus changes, enhancing temporal contrast. In olfaction, odor 3 4 concentration changes across consecutive inhalations ( $\Delta C_l$ ) can guide odor source localization, yet the neural representation of  $\Delta C_t$  has not been studied in vertebrates. We have found that, in 5 the mouse olfactory bulb, a subset of mitral/tufted (M/T) cells represents  $\Delta C_t$ , enhancing 6 7 the contrast between different concentrations. These concentration change responses are 8 direction selective: they respond either to increments or decrements of concentration, reminiscent of ON and OFF selectivity in the retina. This contrast enhancement scales with the magnitude, 9 but not the duration of the concentration step. Further,  $\Delta C_t$  can be read out from the total spike 10 count per sniff, unlike odor identity and intensity, which are represented by fast temporal spike 11 patterns. Our results demonstrate that a subset of M/T cells represents  $\Delta C_t$ , providing a signal 12 that may instruct navigational decisions in downstream olfactory circuits. 13

### Significance

As an animal tracks an odor plume, concentration changes over time. Here we show that olfactory bulb neurons explicitly represent concentration changes between consecutive inhalations. This response property enhances temporal contrast, as in other sensory systems. Fine temporal spike patterns do not improve concentration change decoding. These signals may guide olfactory navigation in the natural environment.

### 19 Introduction

20 The brain must track how external information changes with time (Wertheimer, 1912; Bregman, 1994). Correspondingly, sensory circuits deploy specialized cell types for dynamic stimuli: 21 visual neurons emphasize luminance changes and motion (Ratliff et al., 1963), auditory neurons 22 23 capture amplitude and frequency modulation (Langner, 1992), and somatosensory neurons encode vibrating touch (Werner and Mountcastle, 1965; Mountcastle et al., 1967). For many 24 animals, odor concentration changes are equally relevant, since they carry information about 25 26 odor source location (Murlis et al., 1992; Ache et al., 2016). Vertebrates can localize odor 27 sources either by comparing between simultaneous samples from the two nostrils, or by 28 comparing samples taken sequentially from different locations (Catania, 2013). When bilateral 29 sampling is prevented by naris occlusion, animals are only partly impaired at localizing odor 30 sources (Porter et al., 2007; Khan et al., 2012; Catania, 2013; Jones and Urban, 2018). Therefore, 31 vertebrates must also sense changes of odor concentration, from sniff to sniff  $(\Delta C_l)$ , to guide 32 them to an odor source. Yet despite this evidence that  $\Delta C_t$  can guide odor tracking, whether 33 olfactory neurons encode sniff to sniff changes has not been directly addressed.

Unlike invertebrate olfactory systems, in which olfactory sensory neurons (OSNs) are continuously exposed to the medium, air-breathing vertebrates discretize the input to OSNs into intermittent inhalations. In this case, the brain must maintain a memory of odor concentration across the exhalation interval to compute  $\Delta C_t$ .

How and where does the olfactory system solve this problem? We demonstrate here that a subset 38 of neurons in the olfactory bulb encode  $\Delta C_i$  on the time scale of a single sniff. Thus, like their 39 counterparts in other sensory systems such as ON/OFF responses in vision (KUFFLER, 1953; 40 41 Schiller, 1992; Westheimer, 2007), a subset of olfactory neurons represents stimulus increments and decrements. Further, these representations depend on the magnitude of the concentration 42 43 step, but not the duration of the step (i.e., for how many sniffs it lasts). Lastly, while fast temporal spike patterns can improve decoding of absolute concentration, concentration changes 44 45 can be read out from total spike count.

### 46 Experimental procedures

### 47 Animals

48 Data were collected in seven C57BL/6J male mice. Subjects were 8–16 weeks old at the 49 beginning of recordings and were maintained on a 12-h light/dark cycle (lights on at 8:00 p.m.) in isolated cages in an animal facility. All animal care and experimental procedures were in
accordance with a protocol approved by the University of Haifa and University of Oregon
Institutional Animal Care and Use Committees.

### 53 Surgery

54 Mice were anesthetized using isofluorane gas anesthesia, and a head plate and a pressure cannula were implanted. For sniffing cannula implantation, we drilled a small hole in the nasal bone, into 55 which the thin 7-8 mm-long stainless cannula (gauge 23 capillary tubing, Small Parts) was 56 57 inserted, fastened with glue, and stabilized with dental cement (Verhagen et al., 2007). A small craniotomy was performed above one of the olfactory bulbs, contralateral to the side of sniffing 58 59 cannula implantation. The reference electrode was implanted in cerebellum. At the end of the procedure, the craniotomy was covered with a biocompatible silicone elastomer sealant (Kwik-60 cast, WPI). The mice were given 3 days after a surgery for recovery. 61

### 62 **Odor delivery**

63 For stimulus delivery, we used a custom eight-odor air dilution olfactometer, based on a previous 64 design (Bodyak and Slotnick, 1999). When no odor was being presented to the mouse, a steady 65 stream of clean air (1,000 ml/min) was flowing to the odor port. During odorant presentation, N2 flowed through the selected odorant vial. We used multiple odorants obtained from Sigma-66 Aldrich. The odorants were stored in liquid phase (diluted either 1:5 or 1:10 in mineral oil) in 67 68 dark vials. We used acetophenone, amyl acetate, geraniol, ethyl acetate, S - limonene, methyl butyrate, menthone, methyl salicylate, pentyl acetate and vanillin as odorants. The odorant 69 concentration delivered to the animal was reduced additional tenfold by air dilution and 70 71 homogenized in a long Teflon tube before reaching the final valve. After sufficient mixing and 72 equilibration time, the dual three-way Teflon valve (SH360T042, NResearch) directed the odor 73 flow to the odor port and diverted the clean airflow to the exhaust. All air flows and line impedances were equalized to minimize the pressure transients resulting from odor and final 74 75 valve switching. The time course of odor concentration was checked by Photo-Ionization Detector (200B mini-PID, Aurora Scientific). The concentration reached a steady state ~40 ms 76 77 after final valve opening (Resulaj and Rinberg, 2015). Further, to change odor concentration, we 78 passed stable odorized airflow through a concentration change manifold (Fig. 1a). Odor 79 concentration changes were achieved by activating a pair of matching solenoids (LHQA2411220H; The Lee Company) which performed air dilution. For each pair of solenoids, 80 81 one valve was connected to a vacuum channel and the other to a clean airflow channel. Solenoid

82 activation in the vacuum channel diverted part of the odorized air, while solenoid activation in the air channel contributed an equal amount of flow back into the system. To maintain constant 83 84 total airflow (Extended data Figure 1-1b), the impedance of each air channel was matched to the 85 impedance of the corresponding vacuum channel using manual needle valves R1..3 (NV3H-1012-3-S; Beswick Engineering). To ensure that the temporal profile of odor concentration 86 87 stabilized before inhalation began, we predominantly used odorants with higher vapor pressure 88 (Martelli et al., 2013). For these high vapor pressure odorants, the stimulus reaches 95% of final concentration in 20-40 ms (Fig. 1c). 89

### 90 Electrophysiological recording

91 We recorded M/T cell activity using acute 16- or 128-channel matrix array of Si-probes (a2x2tet-3mm-150-150-121-A16, M4x8-5mm-Buz-200/300um, NeuroNexus). Cells were recorded in 92 93 both ventral and dorsal mitral cell layers. The data were acquired using a 128-channel data 94 acquisition system (RHD2000, Intan Technologies) at 20 KHz sampling frequency. To monitor 95 sniffing, the intranasal cannula was connected to a pressure sensor with polyethylene tubing 96 (801000, A-M Systems). The pressure was measured using a pressure sensor (24PCEFJ6G, 97 Honeywell). The amplified output signal from the pressure sensor was recorded in parallel with 98 electrophysiological data on one of the analog input channels.

99 Before recording began, the mice were first adapted to head fixation. Mice typically remained 100 quiescent after 1-2 sessions of head fixation, after which recording sessions started. We presented 2-3 odors in a single session in pseudo-random sequence with an average inter 101 stimulus interval of 7 s. Each odor was presented in four temporal patterns: 1) static high – high 102 103 concentration (~1-2% of saturated vapor pressure) of odor for 4 sniff cycles; 2) static low – low 104 concentration (50% of high concentration level) for 4 sniff cycles; 3) a step from high to low – 105 for the first two sniff cycles, concentration level was equal to the level of static high, after which the concentration stepped to the low concentration; 4) and a step from low to high – two sniff 106 107 cycles of low concentration followed by two sniffs of high concentration. We controlled odor 108 concentration using a custom-built concentration change manifold (CCM, see next section). Odor onsets and concentration changes were triggered at the beginning of the exhalation phase, 109 110 which occur at positive-going zero crossings of the pressure signal. Since odor cannot orthonasally enter the nose during exhalation, triggering by exhalation onset allows enough time 111 for the odor stimulus to reach a steady state of concentration by the time the animal begins to 112 113 inhale. One session usually lasted for 60-90 min and consisted of 300-400 trials.

### 114 Spike extraction and data analysis

- 115 All analysis was done in Matlab (MathWorks). Electrophysiological data were filtered between
- 116 300 Hz 5 KHz and spike sorted. For spike sorting we used software package written by Alex
- 117 Koulakov (Shusterman et al., 2011).

### 118 Statistical table

	Data structure	Type of test	Power
If cell is responsive to an odor	Fitted data, non- normal	Kolmogorov- Smirnov test	p < 0.005
ROC analysis CI	Fitted data, normal	t-test	p = 0.63
ROC analysis CT	Fitted data, normal	t-test	p = 0.08
ROC analysis +/- $\Delta C_t$	Fitted data, normal	t-test	p < 0.001
Spike count contrast enhancement for $+/-\Delta C_t$	Fitted data, non- normal	W HOOAOH	$p = 7.57e-5 \text{ for } + \Delta C_t \text{ responses}$ $p = 8.64e-5 \text{ for } -\Delta C_t \text{ responses}$
Spike count contrast enhancement for CT	Fitted data, non- normal	Wilcoxon signed rank test	p = 0.20
Spike count contrast enhancement for CI	Fitted data, non- normal	Wilcoxon signed rank test	p = 0.18
Peak amplitude contrast enhancement for $+/-\Delta C_t$	Fitted data, non- normal	W HOOAOH	$p=2.41e-6 \text{ for } + \Delta C_t \text{ responses}$ $p=2.08e-8 \text{ for } -\Delta C_t \text{ responses}$
Peak amplitude contrast enhancement for CT	Fitted data, non- normal	Wilcoxon signed rank test	p = 0.97
Peak amplitude contrast enhancement for CI	Fitted data, non- normal	Wilcoxon signed rank test	p = 0.21
$\Delta C_t$ sensitivity is step magnitude dependent	Normal distribution	t-test	1.25-fold change: p=0.72; 1.5-fold change: p<0.01; 2-fold change: p<0.01
$\Delta C_t$ sensitivity is step duration independent	Normal distribution	Wilcoxon test	for spike count $p = 0.08$ ; for peak amplitude $p = 0.12$

119

### 120 Temporal alignment of responses

121 For analysis, sniffing traces were down-sampled to 1 kHz, and filtered in the range of 0.5–30 Hz. 122 The inhalation onset and offset were detected by zero crossings of a parabola fit to the minima of 123 the pressure signal following the onset of the inhalation. Inhalation onset/offset was defined as 124 the first/second zero crossing of the parabola (Shusterman et al., 2011). We defined two intervals: the first is from inhalation onset to inhalation offset and the second is the rest of the 125 126 sniffing cycle, from the inhalation offset to the next inhalation onset. While the duration of the first interval is concentration independent, the duration of the second interval depends on the 127 concentration of presented odor (Extended data Figure 5). To compare neuronal responses across 128 trials and concentrations, we morphed the inhalation part of the sniff cycle and corresponding 129 spike train to the average one (Shusterman et al., 2011). The second part of the sniff cycle and 130 131 corresponding neural activity were matched to the average over trials: longer cycles were 132 truncated and shorter were zero padded.

### 133 Odor responses.

134 To establish whether a cell is responsive to an odor, we compared the cumulative distribution of 135 the neuronal spikes without odors to the cumulative distribution of neuronal activity during the 136 first odorized sniff cycle, using the Kolmogorov-Smirnov test. Neuronal activity without odor 137 was sampled from 3 sniffs preceding odor delivery across all trials. Neuronal activity for a given odor was sampled from the first sniff after stimulus onset. Cells were considered responsive if 138 139 the distribution of spiking activity during the first odorized cycle statistically differed from the 140 distribution of baseline responses in at least one 10 ms bin relative to inhalation onset (p < 0.005; Benjamini-Hochberg multiple comparison correction) or if their average spike rate over the sniff 141 142 cycle differed significantly from baseline (p < 0.05).

### 143 Recovery index

To measure how  $\Delta$ Ct cell-odor pairs recover in sniffs after the concentration step, we quantified a recovery index (RI), using the peak amplitude of the response. For positive  $\Delta C_t$  responses it consists of the ratio between *change of response between two consecutive sniff cycles after the concentration change* (LH3-LH4) to *the difference between*  $\Delta C_t$  *response and the response on the matching static stimulus (LH3-H3)*:

149

$$\frac{LH3 - LH4}{LH3 - H3}$$

If the M/T cell responds with identical amplitude on two sniff cycles following the concentration step, this will lead to LH4 = LH3, the numerator will be zero and thus RI=0. In the other limiting case, when the response on the second sniff following the step (LH4) is equal to the static response (H3), the denominator will be equal to the numerator and therefore RI will be equal 1. Therefore most of the RIs will be distributed between 0 and 1.

155 By analogy, for negative  $\Delta C_t$  responses, RI will take the following form:

156

## $\frac{HL3 - HL4}{HL3 - L3}$

### 157 ROC analysis of contrast enhancement

ROC analysis provides a measure of how well a given cell-odor pair can discriminate between 158 159 two stimuli. To measure the discriminability between the static odor stimuli, high and low, we compute the area under the ROC curve (auROC) for the distributions of spike counts over the 160 third sniff of each stimulus (Extended Data Figure 4-2 A1, B1, C1; Green and Swets, 1966). 161 162 ROC curves were created by plotting the probability that the single-trial spike count (Extended Data Figure 4-2 A2) exceeds a given value (Extended Data Figure 4-2 A3, B3, C3) for two 163 164 stimulus types. For each point, on the x-axis is the probability for one stimulus type, on the yaxis is the probability for another stimulus type. Dark curves show the probabilities for dynamic 165 versus static, while lighter curves show the probabilities of static high vs static low. An auROC 166 value of 1 indicates no overlap between the two distributions while a value of 0.5 indicates 167 complete overlap between the two distributions. We then plot the static stimulus auROC against 168 the  $\Delta C_t$  discriminability (Extended Data Figure 4-2 D, E). This plot shows whether a given cell-169 170 odor pair shows contrast enhancement between concentrations during step stimuli.

Three example cell-odor pairs are shown in such a plot (Extended Data Figure 4-2, A-C). 171 172 Concentration invariant responses do not discriminate between high and low concentration and 173 have values of near 0.5 for both static and step stimuli. Concentration-tracking responses 174 discriminate between step stimuli and corresponding control equally as well as they discriminate 175 between the two static control stimuli. Thus, they fall along the diagonal of this plot. Finally,  $\Delta C_t$ responses discriminate better between sniffs of step stimuli than for sniffs of static stimuli, so 176 they fall above the diagonal. CI responses do not discriminate between high and low 177 178 concentration (t-test, p = 0.63), and give values of near 0.5 for both static and flickering stimuli (Extended Data Figure 4-2E). CT responses discriminate equally well between static and 179 180 flickering stimuli, and thus fall along the diagonal of this plot (t-test, p = 0.08).  $\Delta C_t$  responses discriminate better between dynamic and static stimuli than between two static stimuli, so that they fall above the diagonal (t-test, p < 0.001 for both  $+\Delta C_t$  and  $-\Delta C_t$ ). These analyses demonstrate that  $\Delta C_t$  sensitivity enhances the contrast between concentrations, potentially facilitating detection of concentration change.

### 185 Odor concentration classification analysis.

186 To estimate how well single neurons (n=49) can discriminate between two odor concentrations on a trial by trial basis, we constructed a Mahalanobis distance linear classifier. For 187 concentration discrimination, we calculated discriminability between responses to static high and 188 static low on the 3<sup>rd</sup> sniff cycle, L<sub>3</sub> and H<sub>3</sub>. For every cell and for every pair of concentrations we 189 counted spikes using multiple time bins (5, 10, 20, 40, 80 and 160 ms). Single trials were 190 randomly selected and compared to a set of templates constructed from 70% of trials for each of 191 192 the two concentrations. We used the *mahal* function in Matlab to estimate Mahalanobis distance 193 from each single trial vector to two groups of multiple trial templates representing two 194 concentrations. This procedure was repeated 300 times for different single trial population 195 vectors and was repeated for each bin size.

A similar analysis was performed on the same cell-odor pairs to estimate discriminability in  $\Delta C_t$ . For  $\Delta C_t$  discrimination we calculated discriminability between LH<sub>3</sub> and L<sub>3</sub> sniffs for  $+\Delta C_t$ responses and HL<sub>3</sub> and H<sub>3</sub> sniffs for  $-\Delta C_t$  responses.

### 199 Behavioral experiments

2 mice were implanted with a head bar and a cannula in their nose, both secured to the skull by
dental cement (Smear et al., 2011). After recovery from surgery, mice were water restricted so
that they are motivated to work for water reward during behavioral testing.

To measure  $\Delta C_t$  sensitivity, we used a go/no-go paradigm (Smear et al., 2011). Trial events were controlled and behavioral outputs (sniffing and licking) were measured using MATLAB and a custom-built Arduino-based behavior-control system. Stimulus presentation is synchronized to the sniff cycle, such that changes in odor concentration only occur while the animal is exhaling. Thus, there is no change in odor concentration during inhalation, and the animal must compare two discrete odor samples across time to detect any changes in odor concentration.

209 Mice were initially trained in a simple odor detection task, in which they are supposed to lick 210 when odor is presented, and not lick when a blank stimulus occurs. After they have acquired at 211 least 90% performance in this task, they begin  $\Delta C_t$  training. In the second phase of training, mice 212 were trained to report positive or negative  $\Delta C_t$  relative to an absolute concentration, C. All trials start by delivering the baseline concentration C to the subject during the first sniff. During the 213 second sniff, however, the concentration can either change ( $C + \Delta C_t$  or  $C - \Delta C_t$ ; No-Go trials) or 214 215 stay at C (Go trials). Trials containing the  $\Delta C_t$  signal are used as No-Go trials, because in a Go/No-go task most errors are false alarms. By delivering  $\Delta C_t$  stimuli during no-go trials, we 216 ensure that the majority of errors occur during  $\Delta C_t$  trials, making these trials more informative. 217 218 Responses are classified into correct - hits (H: Go trial, mouse licks), correct rejections (CR: No-Go trial, mouse doesn't lick) – and incorrect – false alarms (FA: No-Go trial, mouse licks) & 219 misses (M: Go trial, mouse doesn't lick). 220

221 Results

### 222 Experimental setup and response types

We recorded respiration and M/T cell activity (7 mice, 92 cells, 242 cell-odor pairs) in awake, head-fixed mice (Fig. 1A). To rapidly change odor concentration, we developed a novel concentration change manifold, with which rapid concentration changes were achieved by air dilution (Fig. 1A; Methods). Sniffing was measured through an intranasal pressure cannula (Fig. 1A). Using real-time closed-loop odor presentation, we switched odor concentrations at the beginning of the exhalation phase so that the stimulus reached its new steady state concentration before the onset of the next inhalation (Fig. 1B; and Extended data Figure 1-1).

In most experiments, we presented odorants in two static concentration patterns: high (H), low (L), and two dynamic patterns: a step from high to low (HL), and a step from low to high (LH). The high concentration was twice that of the low concentration, a concentration difference that is within the range of concentration changes that would be encountered in turbulent plumes (Crimaldi et al., 2002; Gaudry et al., 2012; Gire et al., 2016). Behavioral testing in a Go/No go paradigm confirmed that two-fold concentration steps are perceptible to mice (Extended data Figure 1-2).

Step stimuli consisted of a presentation of one concentration for two sniff cycles, followed by a switch to the other concentration. These stimuli evoked three different response types across odor-cell pairs. For some cell-odor pairs, spiking responses were proportional to odor concentration on the current sniff but were not affected by odor concentration on previous sniffs. Thus, these concentration-tracking cell-odor pairs (*CT*; Fig. 1C-D) faithfully represented the concentration on each sniff. For other cell-odor pairs, the response did not change across 243 concentrations for static or step stimuli. We refer to these as concentration-invariant (Cl; Fig. 1E-These unchanging responses may be specialized for odor identification, for which 244 F). 245 concentration invariance is an important property (Wilson and Mainen, 2006; Shusterman et al., 246 2017; Wilson et al., 2017; Bolding and Franks, 2018). However, testing with a wider range of 247 concentrations would be needed to fully determine these cells' concentration response function for a given odor. Lastly, we observed responses that were sensitive to changes in odor 248 249 concentration ( $\Delta C_t$ ; Fig. 2). For these cell-odor pairs, responses to step stimuli could not be predicted from responses to static stimuli. These  $\Delta C_t$  cell-odor pairs responded to LH (+ $\Delta C_t$ 250 responses; Fig. 2A-B and Extended data figure 2-1A) or to HL stimuli (- $\Delta C_t$  responses; Fig. 2C-251 252 D and Extended data figure 2-1A). For example, such a cell-odor pair may exhibit an identical 253 response to static high and static low stimuli but respond differently when these same 254 concentrations are alternated in the HL stimuli (Fig. 2C-D). Because of this history dependence, 255 such a response carries information about concentration change rather than the concentration *per* 256 se. The majority of  $\Delta C_t$  responses were selective for the direction of change (41/49; Extended data 257 Figure 2-2). Further, almost all  $\Delta C_t$  responses increased firing rate with positive concentration 258 changes and decreased firing rate with negative changes (46/49). Strikingly, 25% of the  $\pm \Delta C_t$ 259 responses did not respond to the initial stimulus onset (first sniff), a change from no odor to odor, but only after the upward step in concentration (7/28; Fig. 2A). 260

For a cell to reliably report  $\Delta C_t$  with single sniff temporal resolution, its response should only be 261 detectably different in the sniff that immediately follows the concentration change. On the next 262 263 sniff, the response should return to the level evoked by static stimuli. To quantify the extent of 264 recovery to the static level on the second sniff after the concentration change, we devised a recovery index (see Methods and Extended Data Figure 2-3). This index ranges from 1 for 265 266 complete recovery, to 0 for no recovery to the static stimulus response (Fig. 2E-F). While  $\pm \Delta C_t$ responses mostly recovered near to the static level (Fig. 2E),  $-\Delta C_t$  responses do not recover 267 268 completely (Fig. 2F).

All responses were classified as  $\Delta C_i$ , *CT*, or *CI*. To categorize each response, we tested whether the cumulative distribution of spike count after inhalation onset differed between stimuli (Kolmogorov-Smirnov test; Fig. 3A; see Methods). This statistical test is sensitive not only to changes in the total number of spikes within a sniff cycle but also to temporal redistribution of spikes within the cycle. Importantly, due to adaptation, both representation of odor concentration (Cang and Isaacson, 2003; Sirotin et al., 2015) and perception of odor intensity (Wojcik and Sirotin, 2014) depend on the duration of odor exposure. Therefore, for all analyses, we compare responses to different stimuli on the same sniff cycle after stimulus onset (e.g., we compare the 3<sup>rd</sup> sniff of the step stimulus to the 3<sup>rd</sup> sniff of the static stimulus; see Extended Data Figure 2-4 for an example response with strong adaptation).

279 Concentration tracking (CT) responses differ on the first sniff of the static stimuli, but do not differ between the third sniff of step and static stimuli. (Fig. 3B1, C). A cell-odor pair is 280 categorized as concentration invariant (CI) if the response on the first sniff of the static stimuli 281 does not significantly differ between high and low, and the response on the third sniff of the 282 283 concentration step stimulus does not differ from the third sniff of the two static stimuli. (Fig. 284 3B2, C).  $\Delta C_t$  sensitive responses differ on the third sniff of the  $\Delta C_t$  stimulus from the third sniff of both static stimuli. If after a positive change in concentration, the cell responded differently 285 from its response to static high concentration, this cell-odor pair was categorized as  $+\Delta C_t$  (Fig. 286 287 3B3, C).  $-\Delta C_t$  cell-odor pairs gave a different response to the low concentration depending on the concentration in the preceding sniff (Fig 3B4, C). In summary, 51% (n=123) of cell-odor pairs 288 289 responded to the odorants we presented. Of these responsive cell-odor pairs, 41% were  $\Delta C_i$ , 20% were CT and 39% were CI (Fig. 3D). 290

What is the cellular basis of  $\Delta C_t$  sensitivity? Are there dedicated " $\Delta C_t$  cells" that represent 291 292 concentration changes for all their effective odor stimuli, or does  $\Delta C_t$  sensitivity depend on odor 293 identity? To approach this question, we compared the responses of each cell to different odors (Fig. 3E). An individual cell could belong to different response types for different odors. 294 Importantly, cells with  $\Delta C_t$  sensitivity to one odor are not always  $\Delta C_t$  sensitive to other odors at 295 the tested concentrations (Fig. 3E). Therefore,  $\Delta C_t$  sensitivity cannot be invariant to both odor 296 297 identity and concentration. Further studies using a wider range of absolute concentrations will be 298 necessary to determine whether there is invariance to either of these features.

### 299 Contrast between concentrations depends on the stimulation history

In  $\Delta C_t$  responses (Fig. 2), the response to a given concentration depends on the concentration presented in the previous sniff. On the sniff after a concentration change, the difference between responses to different concentrations will be enlarged, thus enhancing the contrast for that sniff. Responses of M/T cells may encode odor stimuli either by changes in spike count or by changes in temporal profile without changes in spike count (Cury and Uchida, 2010; Shusterman et al., 2011). Our method of classifying responses is sensitive not only to changes in the total number 306 of spikes within a sniff cycle but also to temporal redistribution of spikes within the cycle. To 307 separately quantify which features of neuronal responses contribute to contrast enhancement, we 308 compared the difference between responses to high and low concentrations when preceded by a 309 step to the difference when preceded by the same concentration (Fig. 4A). We plotted full sniff spike count differences between the 3<sup>rd</sup> sniffs of the two static stimuli (|High - Low|) against 310 spike count differences between a dynamic step stimulus and the corresponding static stimulus 311 312 (i.e., |Dynamic - Static|). In this visualization, the farther a cell-odor pair is from the diagonal, the stronger its contrast enhancement (Fig. 4B). Both  $+\Delta C_t$  and  $-\Delta C_t$  response populations showed 313 314 contrast enhancement, with responses significantly shifted from the diagonal (Wilcoxon signed rank test, p= 7.57e-5 for  $+\Delta C_t$  and p= 8.64e-5 for  $-\Delta C_t$  responses), while the distributions for CT 315 (Wilcoxon signed rank test, p = 0.20, n=25) and CI (Wilcoxon signed rank test, p = 0.18, n = 49) 316 317 responses are symmetric about the diagonal (Fig. 4C, Extended Data Figure 4-1A).

318 To quantify how  $\Delta C_t$  sensitivity enhances sub-sniff temporal differences between odor responses, 319 we next performed the same comparison for differences in peak amplitude (peak firing rate) (Fig. 320 4D, Extended Data Figure 4-1B), a feature that reflects fast temporal patterning (Cury and Uchida, 2010; Shusterman et al., 2011). Peak amplitude difference distributions for  $\Delta C_t$ 321 322 responses were significantly shifted from the diagonal (Wilcoxon signed rank test, p=2.41e-6 for  $+\Delta C_t$  and p= 2.08e-8 for  $-\Delta C_t$  responses), while for CT and CI responses the distributions were 323 symmetric about the diagonal (Wilcoxon signed rank test, p = 0.97 and 0.21, respectively). Thus, 324  $\Delta C_t$  sensitivity also increased contrast at the faster sub-sniff timescale. Lastly, to determine the 325 trial by trial reliability of contrast enhancement by  $\Delta C_t$  responses, we used receiver operator 326 characteristic (ROC) analysis (see Methods). In this analysis,  $\Delta C_l$  responses discriminated better 327 328 between dynamic and static stimuli than between two static stimuli (Extended Data Figure 4-2). These analyses demonstrate that  $\Delta C_t$  sensitivity enhances the contrast between concentrations, 329 potentially facilitating detection of concentration changes. 330

### 331 $\Delta C_t$ sensitivity is step magnitude dependent

We next tested how  $\Delta C_t$  sensitivity depends on the magnitude of the concentration step. Because two-fold concentration changes are in the range observed in turbulent plumes (Mylne and Mason, 1991; Crimaldi et al., 2002), and because firing rates fell to near zero in some  $-\Delta C_t$ responses (Fig. 2C, Extended data Figure 2-2), we tested responses to smaller concentration steps. In addition to the twofold steps used in the experiments above, we included a 1.5-fold and a 1.25-fold step, both LH and HL (Fig. 5A, D). To quantify  $\Delta C_t$  sensitivity, we took the ratio of the 338 response to the dynamic stimulus to that of the static stimulus, for full sniff spike count as well as peak amplitude of the PSTH.  $+\Delta C_t$  responses (Fig. 5B) were largest for the 2-fold 339 concentration increase, as expressed by the ratio of the response to the 3rd sniff of the dynamic 340 stimulus (LH<sub>3</sub>) to that of the corresponding static stimulus (H<sub>3</sub>), both for spike count and peak 341 342 amplitude (Fig. 5C). Across the population of  $+\Delta C_t$  responses, the two larger steps gave significant increases in spike count (t-test; 1.25-fold change: P=0.72; 1.5-fold change: p<0.01; 2-343 344 fold change: p < 0.01), whereas only the largest step evoked a significant increase in peak amplitude: count (t-test; 1.25-fold change: p=0.5; 1.5-fold change: p=0.06; 2-fold change: 345 p<0.001). For  $-\Delta C_t$  responses (Fig. 5E), spike counts were significantly reduced for all step sizes 346 tested (Fig. 5F; t-test; 1.25-fold change: p<0.01; 1.5-fold change: p<0.001; 2-fold change: 347 p < 0.01), while peak amplitudes were significantly reduced for the two larger steps (Fig. 5F; t-348 349 test; 1.25-fold change: p=0.019; 1.5-fold change: p<0.001; 2-fold change: p<0.001). Thus, larger 350 concentration steps give rise to stronger contrast enhancement.

### 351 $\Delta C_t$ sensitivity is independent of step duration

352 All responses we have shown thus far come from stimuli with steps lasting 2 sniffs. In natural 353 environments, more rapid variations in odor concentration are common (Murlis et al., 1992). To test the extent to which  $\Delta C_t$  sensitivity is also evoked by briefer steps, we performed additional 354 experiments in which concentration changed after one sniff (Fig. 6A). To quantify step duration 355 356 dependent differences in  $\Delta C_t$  sensitivity, we normalized the peak amplitude (Fig. 6B) and spike count (Fig. 6C) of the  $\Delta C_t$  responses to the response for the one sniff step. While some responses 357 were step duration dependent (5/13), across the population the differences were not significant 358 359 (Wilcoxon test; Fig. 6B, p=0.08; Fig 6C, p=0.12). To characterize the extent to which contrast 360 depends on step duration, as above we calculated the ratio of the dynamic response magnitude to 361 static response magnitude for response amplitude (Fig. 6D) and spike count (Fig. 6E) and normalized this value to that of the one sniff long step. Across the population these differences 362 were not significant (Wilcoxon test; Fig 6D, p=0.16; 6E, p=0.41). 363

### 364 Concentration decoding depends on temporal pattern, while $\Delta C_t$ decoding does not

In awake animals, M/T cell activity carries information about odor identity (Cury and Uchida, 2010; Shusterman et al., 2011) and intensity (Sirotin et al., 2015) at sub-sniff timescales. To compare how information about concentrations and about changes in concentration might be decoded by downstream olfactory areas, we performed discriminant analysis (see experimental 369 procedures). We first evaluated the accuracy with which responses to two odor concentrations can be discriminated by cell-odor pairs with a  $\Delta C_t$  response (Fig. 7A). Classification of 370 371 concentrations was performed on concatenated vectors of firing rates with multiple bin sizes: 5, 372 10, 20, 40, 80 and 160 ms. Concentration classification performance depended on bin size: smaller bin sizes yielded better discrimination (one-way ANOVA; p < 0.01; Fig. 7C). Thus, 373 374 information about odor concentration can be read out most accurately from fine timescale 375 temporal patterns. Using the same classification procedure, we next evaluated whether decoding of concentration changes by the same  $\Delta C_t$  cell-odor pairs similarly depends on temporal 376 377 resolution (Fig. 7B). This analysis indicates that decoding of concentration changes is invariant across the full range of bin sizes (one-way ANOVA, p=0.22; Fig. 7C). These findings suggest 378 that downstream neurons decode concentration and  $\Delta C_t$  via different mechanisms. 379

### 380 Discussion

Studies of freely moving animals have established the importance of odor concentration dynamics in guiding olfactory navigation (Khan et al., 2012; Catania, 2013; Jones and Urban, 2018). While these paradigms have revealed behavioral strategies, odor stimuli in an open field cannot currently be precisely controlled or measured. Without precise knowledge of the stimulus, neuronal responses are difficult to interpret. To achieve precise stimulus control, we have developed a novel system for presenting rapidly changing odor concentration stimuli to headfixed mice.

388 Our concentration step stimuli have revealed three response types across cell-odor pairs: 1) concentration tracking (CT) responses, in which firing rate is proportional to odor concentration 389 on the current sniff, irrespective of concentration in past sniffs; 2) concentration invariant (CI) 390 391 responses, in which firing rate does not vary across the range of presented odor concentrations; and 3) concentration change sensitive  $(\Delta C_t)$  responses, in which firing rate depends not only on 392 the currently-sniffed concentration, but also that of the previous sniff. A given M/T cell can give 393 different response types to different odorants. Thus, it does not appear that these response types 394 395 map onto particular cell types.

396  $\Delta C_t$  responses enhance the contrast between different concentrations, both in fine and coarse 397 timescales. This contrast enhancement scales with the concentration step magnitude but does not 398 depend on the duration of the step. Lastly, we show that decoding of concentration steps doesn't depend on the duration of time bins: reading fine timescale features does not improveclassification performance.

Taken together, we have obtained the first evidence that neurons in the mammalian olfactory system represent inter-sniff changes in odor concentration. Such temporal contrast enhancement is widespread in other sensory modalities, consistent with the paramount importance of sensing stimulus dynamics. Furthermore, we find that this representation is already present near the sensory periphery, in the olfactory bulb. Computing  $\Delta C_t$  near the periphery allows the signal to be broadcast to the OB's numerous targets in the cortex.

### 407 Neuronal mechanisms of $\Delta C_t$ sensitivity

Invertebrate olfactory organs sample incoming odors continuously, so that their OSNs are 408 409 directly exposed to gradients of odor concentration (Nagel and Wilson, 2011; Kim et al., 2015; 410 Schulze et al., 2015), as well as intermittent intensity fluctuations found in plumes (Vickers et al., 2001). In contrast, terrestrial vertebrates such as mice sample odors intermittently. In order to 411 412 compare the intensities of the previous and the current inhalation, the animal must preserve a 413 representation of the previous concentration during the exhalation interval. A simple way in which information can persist over time is through history-dependent adaptation. Adaptation 414 415 allows cells to match their limited dynamic range to the distribution of stimulus intensities in the environment (Kohn, 2007). We propose that the function of  $\Delta C_t$  responses is to shift the dynamic 416 417 range of olfactory neurons to increase sensitivity to concentrations close to the recently inhaled 418 stimulus. A similar adjustment of dynamic range has been observed for motion processing in the insect visual system (Fairhall et al., 2001). Mechanistically, shifts in dynamic range may be 419 implemented via intrinsic neuronal properties, such as spike threshold adaptation(Henze and 420 Buzsaki, 2001; Itskov et al., 2011) Alternatively,  $\Delta C_t$  sensitivity may be achieved by circuit 421 mechanisms, such as intrabulbar interactions (Shepherd and Greer, 1998; Wachowiak and 422 423 Shipley, 2006; Burton, 2017) or cortical feedback (Luskin and Price, 1983; Li and Hopfield, 1989; Boyd et al., 2012; Markopoulos et al., 2012; Boyd et al., 2015; Otazu et al., 2015). 424

A cell with  $\Delta C_t$  sensitivity to one odor can have a different response type to another effective odor. This eliminates the possibility that a dedicated population of " $\Delta C_t$  cells" represents  $\Delta C_t$ irrespective of odor identity and absolute concentration. Similarly, malleable stimulus selectivity has been observed in other sensory systems. For example, in the retina, although it is widely accepted that retinal ganglion cells consist of dedicated cell types with selectivity for a particular 430 visual feature, recent work challenges this view (Rivlin-Etzion et al., 2018; Wienbar and Schwartz, 2018). Identified ON or OFF retinal ganglion cells can change their polarity based on 431 stimulation outside the receptive field (Geffen et al., 2007) and ambient light levels(Tikidji-432 433 Hamburyan et al., 2014). Direction-selective ganglion cells can reverse their preferred direction of motion depending on recent stimulus history (Rivlin-Etzion et al., 2012). Thus, even classic 434 "feature detector" cell types of the retina can change their selectivity under different conditions. 435 436 As with other sensory features, understanding  $\Delta C_t$  processing will require a more thorough exploration of stimulus space, in as close to natural conditions as possible. 437

### 438 Potential relevance of $\Delta C_t$ sensitivity in the natural environment

439 Odor concentration gradients are critical for odor source localization (Murlis et al., 1992). Mice 440 must locate odor sources in various airflow conditions, which will largely determine the spatiotemporal statistics of odor concentration. Turbulence disrupts concentration gradients 441 emanating from a distant odor source (Murlis et al., 1990; 1992; Weissburg, 2000). However, 442 even in turbulent flow, gradients, and therefore  $\Delta C_t$ , become increasingly informative closer to 443 444 the source (Justus et al., 2002; Riffell et al., 2008; Gire et al., 2016). Therefore, when following a 445 plume from a nearby source (Catania, 2013; Gire et al., 2016), or when tracking a depositional odor trail (Khan et al., 2012; Jones and Urban, 2018),  $\Delta C_t$  signals can guide the nose. 446

In the real world, there may also be odor fluctuations faster than the inhalation time scale. We 447 448 argue that temporal changes in odor concentration on the sub-sniff scale are not relevant, due to 449 several slow processes. First, based on the physics of the nasal cavity, odor fluctuations will be low pass filtered (Doebelin, 1990). Second, the odorant molecules must transition from air to 450 liquid and diffuse through the mucus (Hahn et al., 1994). Lastly, the flicker fusion frequency of 451 452 mouse OSNs in vitro is 3-5 Hz (Ghatpande and Reisert, 2011). Because of these slow processes, we think it is unlikely that sub-sniff timescale changes in odor concentration are available to the 453 454 olfactory system.

Vertebrates sense gradients by stereo (inter-naris) and serial (inter-sniff) comparisons (Rajan et al., 2006; Catania, 2013). Because the nares are close together, stereo comparison should be most informative near an odor source, where odor gradients are steep. Shallower gradients, farther from a source, may require the inter-sniff comparison, since the distance between sampling locations can be larger than the inter-naris distance (Catania, 2013). In a turbulent environment with noisy gradients (Gire et al., 2016), comparison over more than two sniff cycles may be

461	required. While stereo comparisons have been studied both behaviorally (Rajan et al., 2006;
462	Porter et al., 2007; Catania, 2013) and electrophysiologically (Rajan et al., 2006; Kikuta et al.,
463	2010), the serial component, which should dominate over a wider range of distances, has not
464	been explored. Our study demonstrates a neural representation of $\Delta C_t$ . We propose that this
465	representation contributes to olfactory search in natural olfactory scenes.

### References

- Ache BW, Hein AM, Bobkov YV, Príncipe JC (2016) Smelling Time: A Neural Basis for
   Olfactory Scene Analysis. Trends Neurosci 39:649–655.
- Bodyak N, Slotnick B (1999) Performance of mice in an automated olfactometer: odor detection,
  discrimination and odor memory. Chemical Senses 24:637–645.
- Bolding KA, Franks KM (2018) Recurrent cortical circuits implement concentration-invariant
  odor coding. Science 361:eaat6904.
- Boyd AM, Kato HK, Komiyama T, Isaacson JS (2015) Broadcasting of Cortical Activity to the
  Olfactory Bulb. Cell Reports 10:1032–1039.
- Boyd AM, Sturgill JF, Poo C, Isaacson JS (2012) Cortical Feedback Control of Olfactory Bulb
  Circuits. Neuron 76:1161–1174.
- 476 Bregman AS (1994) Auditory Scene Analysis. MIT Press.
- Burton SD (2017) Inhibitory circuits of the mammalian main olfactory bulb. J Neurophysiol118:2034–2051.
- Cang J, Isaacson JS (2003) In vivo whole-cell recording of odor-evoked synaptic transmission in
  the rat olfactory bulb. Journal of Neuroscience 23:4108–4116.
- 481 Catania KC (2013) Stereo and serial sniffing guide navigation to an odour source in a mammal.
  482 Nature Communications 4:1441–1441.
- 483 Crimaldi JP, Wiley MB, Koseff JR (2002) The relationship between mean and instantaneous
  484 structure in turbulent passive scalar plumes. Journal of Turbulence 3:N14.
- Cury KM, Uchida N (2010) Robust Odor Coding via Inhalation-Coupled Transient Activity in
   the Mammalian Olfactory Bulb. Neuron 68:570–585.
- 487 Doeblin, EO (1990) Measurement systems: application and design. McGraw-Hill.
- Fairhall AL, Lewen GD, Bialek W, van Steveninck R (2001) Efficiency and ambiguity in an
  adaptive neural code. 412:787–792.
- Gaudry Q, Nagel KI, Wilson RI (2012) Smelling on the fly: sensory cues and strategies for
  olfactory navigation in Drosophila. Curr Opin Neurobiol 22:216–222.
- Geffen MN, de Vries SEJ, Meister M (2007) Retinal ganglion cells can rapidly change polarity
   from Off to On. PLoS Biol 5:e65.
- Ghatpande AS, Reisert J (2011) Olfactory receptor neuron responses coding for rapid odour
   sampling. The Journal of Physiology 589:2261–2273.
- Gire DH, Kapoor V, Arrighi-Allisan A, Seminara A, Murthy VN (2016) Mice Develop Efficient
   Strategies for Foraging and Navigation Using Complex Natural Stimuli. Current Biology:1–14.

- 498 Green DM, Swets JA. (1966) Signal detection theory and psychophysics. Wiley
- Hahn I, Scherer PW, Mozell MM (1994) A mass transport model of olfaction. J Theor Biol
  167:115–128.
- Henze DA, Buzsaki G (2001) Action potential threshold of hippocampal pyramidal cells in vivo
   is increased by recent spiking activity. Neuroscience 105:121–130.
- 503 Itskov V, Curto C, Pastalkova E, Buzsaki G (2011) Cell Assembly Sequences Arising from
- Spike Threshold Adaptation Keep Track of Time in the Hippocampus. Journal of Neuroscience31:2828–2834.
- Jones PW, Urban NN (2018) Mice follow odor trails using stereo olfactory cues and rapid sniff
   to sniff comparisons. bioRxiv:1–24.
- Justus KA, Murlis J, Jones C, Cardé RT (2002) Measurement of Odor-Plume Structure in a Wind
   Tunnel Using a Photoionization Detector and a Tracer Gas. Environmental Fluid Mechanics
   2:115–142.
- Khan AG, Sarangi M, Bhalla US (2012) Rats track odour trails accurately using a multi-layered
   strategy with near-optimal sampling. Nature Communications 3:703–703.
- 513 Kikuta S, Sato K, Kashiwadani H, Tsunoda K, Yamasoba T, Mori K (2010) From the Cover:
- Neurons in the anterior olfactory nucleus pars externa detect right or left localization of odor
   sources. Proc Natl Acad Sci USA 107:12363–12368.
- Kim AJ, Lazar AA, Slutskiy YB (2015) Projection neurons in Drosophilaantennal lobes signal
  the acceleration of odor concentrations. eLife 4:1–27.
- Kohn A (2007) Visual adaptation: physiology, mechanisms, and functional benefits. J
  Neurophysiol 97:3155–3164.
- Kuffler SW (1953) Discharge patterns and functional organization of mammalian retina. J
   Neurophysiol 16:37–68.
- 522 Langner G (1992) Periodicity coding in the auditory system. Hear Res 60:115–142.
- Li Z, Hopfield JJ (1989) Modeling the olfactory bulb and its neural oscillatory processings. Biol
  Cybern 61:379–392.
- 525 Luskin MB, Price JL (1983) The topographic organization of associational fibers of the olfactory
- system in the rat, including centrifugal fibers to the olfactory bulb. Journal of ComparativeNeurology 216:264–291.
- Markopoulos F, Rokni D, Gire DH, Murthy VN (2012) Functional Properties of Cortical
   Feedback Projections to the Olfactory Bulb. Neuron 76:1175–1188.
- 530 Martelli C, Carlson JR, Emonet T (2013) Intensity Invariant Dynamics and Odor-Specific
- Latencies in Olfactory Receptor Neuron Response. J Neurosci 33:6285–6297.

- Mountcastle VB, Talbot WH, Darian-Smith I, Kornhuber HH (1967) Neural basis of the sense of
   flutter-vibration. Science 155:597–600.
- Murlis J, Elkinton JS, Carde RT (1992) Odor plumes and how insects use them. Annu Rev
  Entomol 37:505–532.
- Murlis J, Willis MA, Carde RT (1990) Odour signals: patterns in time and space. Proceedings of
  the Tenth International Symposium on Olfaction and Taste. GCS A/S, Oslo, Norway.
- Mylne KR, Mason PJ (1991) Concentration fluctuation measurements in a dispersing plume at a
  range of up to 1000 m. Quarterly Journal of the Royal Society 117:177–206.
- Nagel KI, Wilson RI (2011) Biophysical mechanisms underlying olfactory receptor neuron
   dynamics. Nat Neurosci.
- Otazu GH, Chae H, Davis MB, Albeanu DF (2015) Cortical Feedback Decorrelates Olfactory
  Bulb Output in Awake Mice. Neuron 86:1–18.
- Porter J, Craven B, Khan RM, Chang S-J, Kang I, Judkewitz B, Judkewicz B, Volpe J, Settles G,
  Sobel N (2007) Mechanisms of scent-tracking in humans. Nature Neuroscience 10:27–29.
- 546 Rajan R, Clement JP, Bhalla US (2006) Rats smell in stereo. Science 311:666–670.
- Ratliff F, Hartline HK, Miller WH (1963) Spatial and temporal aspects of retinal inhibitory
  interaction. J Opt Soc Am 53:110–120.
- Resulaj A, Rinberg D (2015) Novel Behavioral Paradigm Reveals Lower Temporal Limits on
  Mouse Olfactory Decisions. J Neurosci 35:11667–11673.
- Riffell JA, Abrell L, Hildebrand JG (2008) Physical Processes and Real-Time Chemical
  Measurement of the Insect Olfactory Environment. J Chem Ecol 34:837–853.
- Rivlin-Etzion M, Grimes WN, Rieke F (2018) Flexible Neural Hardware Supports Dynamic
   Computations in Retina. Trends Neurosci 41:224–237.
- Rivlin-Etzion M, Wei W, Feller MB (2012) Visual Stimulation Reverses the Directional
   Preference of Direction-Selective Retinal Ganglion Cells. Neuron 76:518–525.
- 557 Schiller PH (1992) The ON and OFF channels of the visual system. Trends Neurosci 15:86–92.
- 558 Schulze A, Gomez-Marin A, Rajendran VG, Lott G, Musy M, Ahammad P, Deogade A, Sharpe
- 559 J, Riedl J, Jarriault D, Trautman ET, Werner C, Venkadesan M, Druckmann S, Jayaraman V,
- Louis M (2015) Dynamical feature extraction at the sensory periphery guides chemotaxis. eLife
   4:e06694.
- 562 Shepherd GM, Greer CA (1998) Olfactory bulb. In G. M. Shepherd (Ed.), *The synaptic* 563 *organization of the brain* (pp. 159-203). New York, NY, US: Oxford University Press.
- Shusterman R, Sirotin YB, Smear MC, Ahmadian Y, Rinberg D (2018) Sniff invariant odor
   coding. eNeuro 2(6) ENEURO. 0149-18.2018.

- eNeuro Accepted Manuscript
- 566 Shusterman R, Smear MC, Koulakov AA, Rinberg D (2011) Precise olfactory responses tile the 567 sniff cycle. Nature Neuroscience 14:1039–1044.
- Sirotin YB, Shusterman R, Rinberg D (2015) Neural Coding of Perceived Odor Intensity.
  eNeuro 5(6) ENEURO. 0083-15.2015.
- Tikidji-Hamburyan A, Reinhard K, Seitter H, Hovhannisyan A, Procyk CA, Allen AE, Schenk
  M, Lucas RJ, Münch TA (2014) Retinal output changes qualitatively with every change in
  ambient illuminance. Nat Neurosci 18:66–74.
- Verhagen JV, Wesson DW, Netoff TI, White JA, Wachowiak M (2007) Sniffing controls an
  adaptive filter of sensory input to the olfactory bulb. Nat Neurosci 10:631–639.
- Vickers NJ, Christensen TA, Baker TC, Hildebrand JG (2001) Odour-plume dynamics influence
  the brain's olfactory code. 410:466–470.
- Wachowiak M, Shipley MT (2006) Coding and synaptic processing of sensory information in the
  glomerular layer of the olfactory bulb. Seminars in Cell & Developmental Biology 17:411–423.
- Weissburg MJ (2000) The fluid dynamical context of chemosensory behavior. Biol Bull198:188–202.
- Werner G, Mountcastle VB (1965) Neural activity in mechanoreceptive cutaneous afferents:
  stimulus\_response relations, weber functions, and information transmission. J Neurophysiol
  28:359–397.
- 584 Wertheimer M (1912) Experimentelle Studien über das Sehen von Bewegung.
- Westheimer G (2007) The ON–OFF dichotomy in visual processing: From receptors to
   perception. Progress in Retinal and Eye Research 26:636–648.
- Wienbar S, Schwartz GW (2018) The dynamic receptive fields of retinal ganglion cells. Progress
  in Retinal and Eye Research:1–0.
- Wilson CD, Serrano GO, Koulakov AA, Rinberg D (2017) A primacy code for odor identity.
  Nature Communications:1–10.
- Wilson RI, Mainen ZF (2006) Early events in olfactory processing. Annu Rev Neurosci 29:163–
  201.
- Wojcik PT, Sirotin YB (2014) Single Scale for Odor Intensity in Rat Olfaction. Current Biology
   24:568–573.
- 595 596

### 597 Figure 1. Concentration tracking and concentration invariant odor responses.

598 A. Schematic of the experiment. Right: A head-fixed mouse implanted with an intranasal 599 cannula and a multi-electrode chamber was positioned in front of the odor delivery port. Left: 600 concentration change manifold. B. Odor concentration step paradigm. Odor concentration changes every two sniff cycles. Green curve indicates the response of a photoionization detector 601 602 (PID) to presentation of ethyl acetate. Sniff waveforms (black) are shown below the plots. Grey 603 areas indicate inhalation. Vertical dashed lines indicate onset of concentration changes. C.-D. Examples of concentration tracking (CT) responses from two cells. Raster and PSTH plots of 604 M/T cell response to static high concentration (orange), static low concentration (blue) and 605 concentration step stimuli (black). The responses of these cell odor pairs change with odor 606 607 concentrations the same way in both static and step stimuli. Bar graph on right shows peak 608 response amplitudes on the third sniff cycle for each stimulus. Error bars indicate standard deviation (see Methods). E.-F. Same as C-D, but for two cell-odor pairs that are invariant to odor 609 610 concentration in the presented range.

611

### **Figure 2.** M/T cells responsive to changes in odor concentration.

613 A, B. Examples of  $+ \Delta C_t$  responses. Raster and PSTH plots of two M/T cell's responses to static high concentration (orange), static low concentration (blue) and low to high (black). Bar graph 614 on right shows peak response amplitudes on the third sniff cycle for each stimulus. Error bars 615 616 indicate standard deviation. C, D. Examples of -  $\Delta C_t$  responses. Raster and PSTH plots of two M/T cell's responses to static high concentration (orange), static low concentration (blue) and 617 618 high to low stimulus (black). E, F. Distribution of recovery indices for  $+ \Delta C_t$  and  $- \Delta C_t$  responses, respectively. A value of 1 indicates complete recovery to the static odor stimulus response, while 619 a value of 0 indicates no recovery. 620

621

### 622 Figure 3. Categorization of response types.

A. Criteria for determining whether a cell was responsive to a given odor. Top: Example of
excitatory odor response PSTH. The black line is a PSTH of spiking during odorized sniffs. The
grey line is a PSTH during unodorized sniffs. Bottom: cumulative spike counts of data from top
plot. The red line indicates the first moment when cumulative distributions with and without

627 stimulus become statistically different. B1-4. PSTHs from examples of each response type to high, low, and low->high stimuli are vertically separated. Arrows indicate which sniffs of the 628 response are statistically compared. Non-significant differences are marked ns, and significant 629 630 differences are marked with \* (Kolmogorov-Smirnov test, p<0.01). B1. A CT cell-odor pair responded differently to the two concentrations, and this difference is not affected by a 631 concentration step. Example data are the same as Fig. 1D. B2. A CI cell-odor pair responded 632 633 identically to both concentrations, with or without a step. Example data are the same as Fig. 1F. **B3.**  $\Delta C_l$  cell-odor pairs responded differently to a given concentration after a concentration step. 634 635 Example data are the same as Fig 2B. B4. Example  $-\Delta C_t$  response data are the same as Fig 2C. C. Comparisons used to categorize odor-cell pairs. D. Distribution of different response 636 types: Concentration Invariant (CI; n=49), Concentration Tracking (CT; n=25), Positive  $\Delta C_t$ 637  $(+\Delta C_t, n=28)$ , and Negative  $\Delta C_t$  (- $\Delta C_t$ ; n=21). E. Distribution of responses to a second odor 638 for positive  $\Delta C_t$  (orange), negative  $\Delta C_t$  (purple), CI (black), and CT (green) cell-odor pairs. 639

640

### 641 Figure 4. Contrast between concentrations depends on the stimulus history.

642 A. Schematic of contrast comparison. To compare contrasts, for each cell-odor pair, we take the difference in response between the 3<sup>rd</sup> sniffs of the static high (H) and static low (L) stimuli, and 643 plot that against the difference between the 3<sup>rd</sup> sniffs of the dynamic stimulus and the 644 corresponding static stimulus (in this example L). Thus, only the concentration in the preceding 645 sniff varies, and the concentrations being compared are constant. B. Expected distribution of 646 647 responses. CT responses will be distributed along diagonal, CI responses will be distributed near 648 the origin, and  $\Delta C_t$  responses will be distributed above diagonal. C. Scatter plot of full sniff spike count differences between two static stimuli against differences between dynamic and static 649 stimuli, on the 3<sup>rd</sup> sniff cycle. CI, CT,  $+\Delta C_t$  and  $-\Delta C_t$  are marked by black, green, orange, and 650 blue color, respectively. Example cells from Fig. 3B1-4 are indicated by enlarged dots. 651 Adjacent panel shows the means and STDs of the spike count differences. D. Same as (C) for 652 653 differences in the peak amplitude of the response. Example cells from Fig. 3B1-4 are indicated 654 by enlarged dots. Adjacent panel shows the means and STDs of the peak amplitude differences. 655 See also Extended Data Figure 4-2.

656

## Figure 5. Contrast enhancement is proportional to the magnitude of concentration changestep.

A. Stimulation with positive steps of different size. B. Raster plots of M/T cell's activity during
L static and three LH dynamic step stimuli. C. Normalized changes in spike count and amplitude
of the response as function of step size. Orange lines are normalized changes for specific cellodor pairs, black line is the mean+/-std change across all responsive cell-odor pairs. Asterisks
mark statistically significant deviations from 1. D-F. Same for negative steps.

664

## Figure 6. Contrast enhancement is independent of the duration of concentration changestep

667 **A.** Example of  $+\Delta C_t$  response to two stimuli of different step durations. Raster and PSTH plots of M/T cell response to static high concentration (orange), static low concentration (blue), low to 668 high, step duration 1 sniff (brown), and low to high, 2 sniffs duration (black). PSTH of response 669 670 for high static stimulus is not shown for clarity of visualization. B. and C. Normalized changes in spike count and amplitude of the  $+\Delta C_t$  responses as function of step duration. Orange lines are 671 normalized changes for  $+\Delta C_t$  responses, purple lines are for  $-\Delta C_t$  responses. Asterisks mark 672 responses for which the 1 sniff step response and the 2sniff step response differ significantly. D. 673 and E. Same as (B and C) for changes in contrast (|Dynamic-Static|). 674

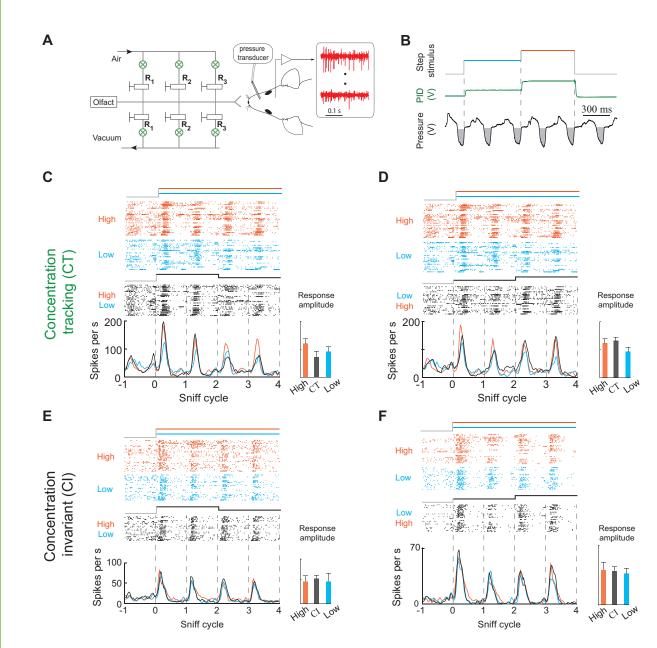
675

### Figure 7. Discrimination among concentrations and changes in concentration by individual M/T cells.

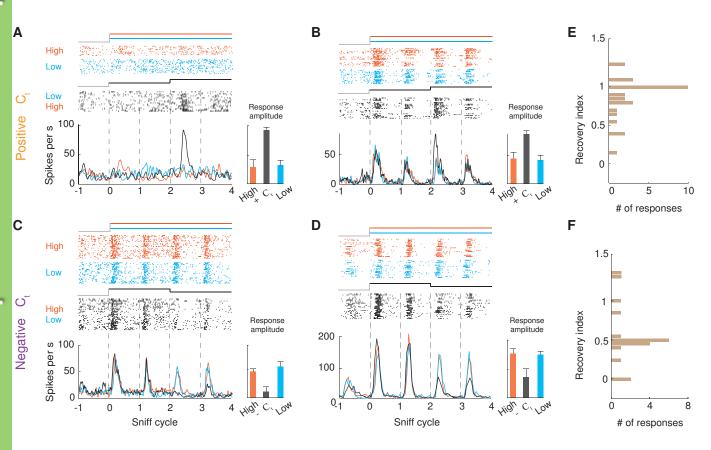
678 A. Top: PSTHs for a single neuron's responses to two static stimuli (red: high concentration, 679 blue: low concentration). Bottom: Corresponding static stimuli discrimination success as a function of time. Vertical dashed lines indicate the end of the inhalation interval. Horizontal 680 681 dashed lines indicate chance level performance. Different colored traces indicate discrimination success for different bin sizes. B. Top: PSTHs for a neuron's responses to a high concentration 682 683 static stimulus (red), and to a positive concentration step (black). Bottom: Corresponding static stimulus vs step stimulus discrimination success as a function of time. Different colored traces 684 indicate discrimination success for different bin sizes. C. Discrimination performance of a linear 685 classifier between two odor concentrations (left) and between changes in concentration (right) 686

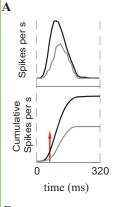
over the 320 ms window, as a function of bin size. Grey lines are performances of individual
neurons. Black line is mean +/- std. Asterisk (\*) indicates significant change (one-way ANOVA;
p<0.01) in discrimination success as function of bin size.</li>

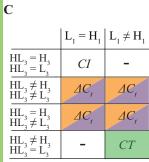
# eNeuro Accepted Manuscript

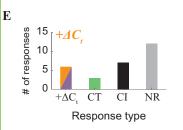


# eNeuro Accepted Manuscript

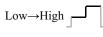






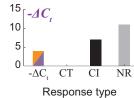




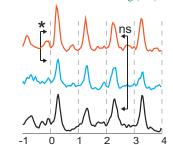


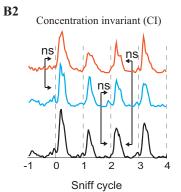
D





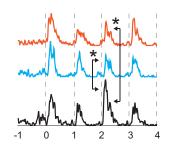


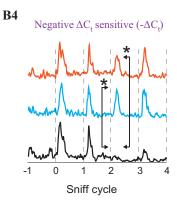


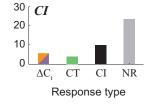


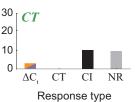
**B3** 

Positive  $\Delta C_t$  sensitive  $(+\Delta C_t)$ 









# eNeuro Accepted Manuscript

